Chiral limits and effect of light on the Hofstadter butterfly in twisted bilayer graphene

Nadia Benlakhouy,[1] Ahmed Jellal,[1,2] Hocine Bahlouli,[3] and Michael Vogl[3,*]

[1]*Laboratory of Theoretical Physics, Faculty of Sciences, Chouaïb Doukkali University, PO Box 20, 24000 El Jadida, Morocco*

[2]*Canadian Quantum Research Center, 204-3002 32 Ave Vernon, BC Canada V1T 2L7*

[3]*Physics Department, King Fahd University of Petroleum & Minerals, Dhahran 31261, Saudi Arabia*

(Received 18 January 2022; revised 23 February 2022; accepted 23 March 2022; published 31 March 2022)

We study the magnetic field induced Hofstadter butterfly in twisted bilayer graphene (TBG) in various kinds of situations. First, we study the equilibrium case and identify the interlayer hopping processes that are most crucial for the appearance of a Hofstadter butterfly. Surprisingly, the hopping processes that are important for the appearance of the Hofstadter butterfly can be categorized as AA stacking type, that is, interlayer hoppings between equivalent sublattices. This is in contrast to AB/BA-type hoppings that are important for the appearance of flat bands in magic angle TBG and were discussed by G. Tarnopolsky, A. J. Kruchkov, and A. Vishwanath [Phys. Rev. Lett. **122**, 106405 (2019)]. We also find that if AB-type interlayer-hopping processes are turned off, the resulting model is chiral but differs from the model discussed mentioned above. Therefore TBG has two separate chiral limits: One of them is important to understand the formation of flat bands and the other for the Hofstadter butterfly. Taking this as motivation we discuss how the role of AA-type hoppings in combination with lattice relaxation effects can make individual Landau levels slightly harder to resolve in an experimental setting than one would expect from a nonrelaxed lattice setting. Finally, we consider the impact of different forms of light on the fractal structure of the butterfly spectrum. Particularly, we study the impact of circularly polarized light and longitudinal light originating from a waveguide. As the system is exposed to circularly polarized light we find butterflies with increasingly pronounced asymmetry with respect to energy $E = 0$. This is due to the introduction of a gap term that breaks the chiral symmetries for both of the two chiral limits mentioned above. Lastly, we study the effect of longitudinal light that can be produced at the exit of a waveguide, in a slightly simplified model. Here, we find that no additional terms that break chiral symmetry are introduced. Therefore it is found to lead to no increase in asymmetry of the energy spectrum. In fact, we identify specific experimentally accessible driving regimes in which the TBG achieves any of the two chiral limits.

DOI: 10.1103/PhysRevB.105.125423

I. INTRODUCTION

The developments that led to our present work go all the way back to graphene, a material that was first synthesized when it was peeled off a graphite substrate using a scotch tape technique [1]. It can be viewed as a monolayer of carbon atoms arranged in a honeycomb crystal lattice structure. This seemingly simple structure is at the origin of marvelous electronic and optical properties that made scientist predict that graphene might revolutionize the nanotechnology industry due to its potential for the development of more efficient electronic components [2]. Indeed, one of graphene's most exciting and counter intuitive transport properties is that is it allows for Klein tunneling: Charges can tunnel through an electrostatic barrier regardless of its height. This effect while it is interesting from a perspective of power consumption has a huge drawback because it means that electrons are difficult to confine. Hence, it thus far—in the case of graphene—prohibits the realization of switching devices such as field effect transistors (FET) which are the basic building blocks of modern electronics. Therefore a lot of efforts have been devoted to overcome this difficulty via band engineering [3–8]. One of the simplest approaches to modify graphene's band structure is by stacking multiple graphene layers on top of one another. The simplest case is different stacking configurations of bilayer graphene (BLG) which consists of two stacked single layers. Bilayer graphenes have continued to attract significant theoretical interest in recent years [9–19].

Recent technological advances have made it possible to tune the electronic properties of layered materials without changing the atomic structure of the individual layers. The simplest technique in this regard is twisting successive layers with respect to one another. Such a twist creates an angle-dependent moiré pattern, a periodic pattern of relatively giant unit cells—a size ∼1000 times the size of AB bilayer graphene's unit cells is not atypical. Moreover, the twist angle plays the role of a knob that affects the carrier interaction. In fact, it has been discovered that at certain, so-called magic angles, flat energy bands occur which then give rise to a plethora of highly correlated phases. An exciting example is a superconducting phase that occurs at the first magic twist angle [20–33]. This superconducting state was first discovered in a land-mark paper in Nature [20]. We stress that this observation can be traced back to the appearance of moiré patterns, which are the source of flat band behavior that eventually gives rise

*ssss133@googlemail.com

 ©2022 American Physical Society

to superconductivity in twisted bilayer graphene (TBLG). It should be mentioned that it was found early on—using scanning tunneling microscope (STM) techniques [34–40]—that these moiré-type patterns can exist in multilayer graphene. Thus, twisted bilayer graphene not only offers the possibility to engineer the electronic band structure but also allows to control the relative importance of carrier correlations.

Last, but not least, band structures can also be modified by the application of periodically time-dependent external drives [33,41–44]. In fact, for the case of graphene it has been shown theoretically that the drastic effect of strong high-frequency electromagnetic fields on the electron energy spectrum near the Dirac point depends strongly on polarization of the field. Linear polarization results in an anisotropic gapless energy spectrum while circular polarization gives rise to an isotropic energy gap. Hence, the transport properties of electrons also in twisted bilayer graphene are strongly affected by the polarization of the electromagnetic waves. From the application point of view, it is easier to control light intensity and polarization of an external light source than the twisting angle. Therefore light can be seen as an ideal control knob for the transport properties of twisted bilayer systems.

Floquet theory has been widely adapted to treat the electromagnetic interaction between external light sources and materials and make these types of predictions. In this context, various techniques have been developed to achieve a time-independent description [45–57]. More recently, the moiré and Floquet approaches have been combined to make theoretical predictions about various topological phases in moiré materials [39,58–62].

Important for our current investigation is the recent work of some of the current authors who studied TBLG under the influence of two distinct forms of light polarization, circularly polarized light and transverse magnetic (TM) light emanating from a waveguide [51,60]. For the circularly polarized light case a rotating frame Hamiltonian, valid for both weak and strong drives in the high to intermediate drive frequency regime, has been developed [51]. This Hamiltonian is appropriate in the regimes where the ordinary Van Vleck approximation (vV) breaks down, and results in a significantly enhanced approximation to the quasienergies [45].

In the present work, we wish to build on these developments and apply the effective Hamiltonian approach [51,60] to another interesting phenomenon that have been investigated in the context of twisted bilayer graphene since the start of this field [63] and has recently begun to rise to popularity again [64–67]. In particular, we consider the so-called Hofstadter butterfly phenomenon [68], where electrons under the influence of a magnetic field exhibit an energy spectrum that displays fractal patterns. These types of fractal butterfly spectra have been observed experimentally in monolayer graphene (MLG) [69,70], in AB-BLG, placed on a hexagonal boron nitride (hBN) substrate [71], also on square, honeycomb and triangular lattices [72,73], kagome lattices [74], and in TBLG [65,67,75,76]. While the effect of a periodic drive - in our case light—on the Hofstadter butterfly has been studied in various systems [3,77–84]. To our knowledge, the Hofstadter butterfly in TBLG has not been extensively studied. Specifically, previous works have mostly focused on the kicked-Harper model [3,77–79]. Other cases include MLG subjected to a uniform perpendicular magnetic field B in combination with a laser. Here, the Floquet Hofstadter butterfly exhibits a richer structure than in the equilibrium case [82–84]. While not extensively studied in TBLG there have been some studies that investigated the Hofstadter butterfly under the influence of light [85,86]. While these works studied extensively the fractal properties of Landau levels under the influence of light, here we want to take a slightly different route and study the interplay between light, chiral symmetries and the fractal properties.

The work is organized as follows. In Sec. II A, we describe TBLG, introduce the theoretical model, and highlight some of its equilibrium properties. In Sec. II B, we analyze which of TBLG's hopping processes is most important for the appearance of a Hofstadter butterfly at low energies and how the different hopping processes influence the symmetry with respect to energy $E = 0$. By inspection of the symmetry properties in twisted bilayer graphene, we find that it has two separate chiral limits. In Sec. III, we describe the first form of light—circularly polarized light—which is used in the Hamiltonian description, and discuss our numerical results. In Sec. IV, we consider longitudinal light emanating from a waveguide and discuss our numerical results. In Sec. V, we summarize our main results and present our conclusions.

II. EQUILIBRIUM CASE

A. Model

We start by considering the simplest case where two graphene layers are miss-aligned with respect to each other by an angle θ. For this work we will work with a model that is valid for $\theta \lesssim 10^\circ$ and will focus on the case of $\theta = 2^\circ$, which lies well within its range of validity. The structure of the lattice we consider can be seen in Fig. 1(a).

Following the approach used in Refs. [63,75,87–90], the Hamiltonian describing TBLG is given by

$$H(\mathbf{x}) = \begin{pmatrix} h(-\theta/2) & T(\mathbf{x}) \\ T^\dagger(\mathbf{x}) & h(\theta/2) \end{pmatrix}, \tag{1}$$

where the intralayer Hamiltonian is given by

$$h(\theta) = v_F \boldsymbol{p} \cdot \boldsymbol{\sigma}_\theta \tag{2}$$

and rotated Pauli matrices are defined by

$$\boldsymbol{\sigma}_\theta = (\cos\theta\sigma_x - \sin\theta\sigma_y, \cos\theta\sigma_x + \sin\theta\sigma_y). \tag{3}$$

The interlayer Hamiltonian describing the tunneling processes between layers is given by

$$T(\mathbf{x}) = \sum_{j=1}^{3} T_j \exp(-i\boldsymbol{q}_j \cdot \mathbf{x}), \tag{4}$$

where $\boldsymbol{q}_1 = k_\theta(0, -1)$, $\boldsymbol{q}_2 = k_\theta(\sqrt{3}, 1)/2$, $\boldsymbol{q}_3 = k_\theta(-\sqrt{3}, 1)/2$ are the nearest neighbor vectors of the moiré Brillouin zone. The characteristic momentum-scale in the moiré Brillouin zone is set by $k_\theta = 2k_D \sin(\theta/2)$ with $k_D = 4\pi/3a_0$ being the Dirac momentum, and $a_0 = 2.46$ Å is

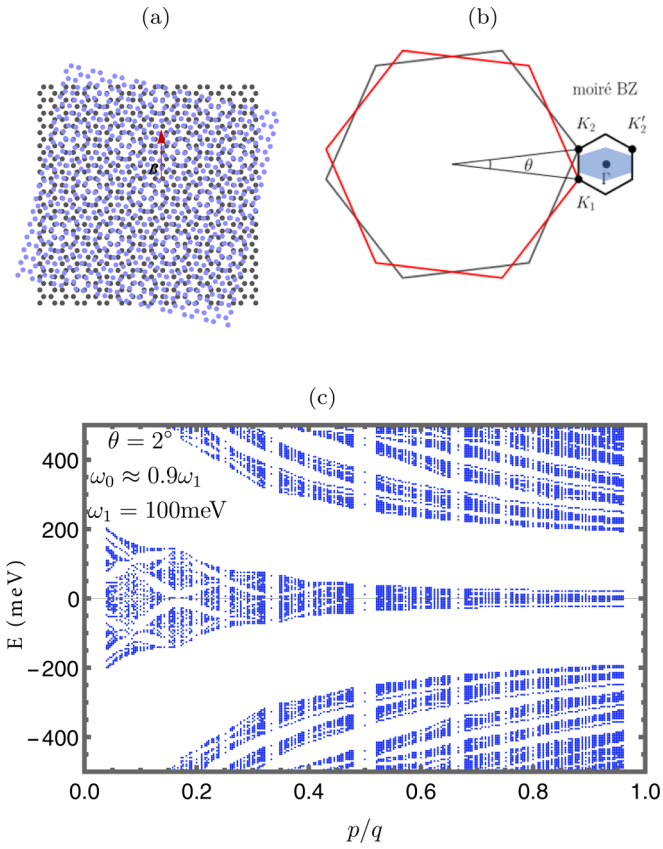

FIG. 1. (a) A sketch of twisted bilayer graphene (TBLG). (b) The moiré Brillouin zone and a schematic depiction of the corresponding magnetic Brillouin zone in blue, which was obtained by reshaping the moiré Brillouin zone in Eq. 14. (c) The Hofstadter butterfly in TBLG.

the lattice constant. The hopping matrices T_i can be expressed in terms of Pauli matrices

$$T_1 = w_0\sigma^0 + w_1\sigma^x, \tag{5}$$

$$T_2 = w_0\zeta^*\sigma^0 + w_1\sigma^+ + w_1\zeta\sigma^-, \tag{6}$$

$$T_3 = w_0\zeta\sigma^0 + w_1\sigma^+ + w_1\zeta^*\sigma^-, \tag{7}$$

where $\zeta = e^{2\pi i/3}$ and $\sigma^\pm = (\sigma^x \pm i\sigma^y)/2$ act on sublattice degrees of freedom. The 2×2 Pauli matrices and identity matrix are denoted by $\sigma^{x,y,z}$ and σ^0, respectively.

We stress that the Hamiltonian introduced here is valid for the moiré BZ that is located near the K point. The Hamiltonian describing the bands near the K' point is related by time reversal symmetry or equivalently it can be obtained by the replacements

$$\begin{aligned} &\mathbf{q}_i \to -\mathbf{q}_i; \quad \zeta \to \zeta^*, \\ &\boldsymbol{\sigma}_\theta \to (-\cos\theta\sigma_x - \sin\theta\sigma_y, -\cos\theta\sigma_x + \sin\theta\sigma_y), \end{aligned} \tag{8}$$

which was also noted in Appendix A of Ref. [91]. We note that for the main part of the paper we will focus on the K point to keep our discussion more coherent. Although, we found it instructive to provide results for the K' point in Appendix .

A few comments are in order about the parameters w_i. Some stacking configurations in TBLG are more energetically favorable than others. Most importantly AB and BA stacking is energetically preferred compared to AA stacked regions [92,93]. This leads to different sizes of AA and AB stacked regions—at very small twist angles AB stacked regions grow in size compared to AA stacked regions [92,93]. Furthermore, the different stacking regions have differing interlayer lattice spacings. We account for these effects in an approximate fashion through the parameters w_i in the interlayer tunneling terms [60,94]. In our specific case we take the hopping amplitudes as $w_0 \approx 90$ meV for AA-type hoppings and $w_1 \approx 100$ meV for AB/BA-type hoppings.

Next, let us discuss this Hamiltonian in the presence of a perpendicular magnetic field $\boldsymbol{B} = B_z\hat{z}$. This type of field is introduced through the minimal substitution procedure $\hat{\boldsymbol{p}} \longrightarrow \hat{\boldsymbol{p}} + e\boldsymbol{A}$. For computational convenience we select the Landau gauge $\boldsymbol{A} = B(-y, 0, 0)$. In this case, we find that the intralayer blocks of our Hamiltonian can be written in terms of ladder operators defined by

$$a = \frac{\ell}{\sqrt{2}}[p_x - eBy - ip_y], \quad a^\dagger = \frac{\ell}{\sqrt{2}}[p_x - eBy + ip_y], \tag{9}$$

which fulfill the usual commutation relation $[a, a^\dagger] = 1$. In this case, the intralayer Hamiltonian becomes

$$h(\theta/2) = \omega_c[\sigma^+ e^{i\theta/2}a + \sigma^- e^{-i\theta/2}a^\dagger], \tag{10}$$

where the $\omega_c = \sqrt{2}v_F/\ell$ is the cyclotron energy, and $\ell = 1/\sqrt{eB}$ is the magnetic length.

Since the dominant energy scale is given by the intralayer contributions it is now convenient to express the full Hamiltonian in a basis of layer index $L = 1$ and 2, sublattice index $\alpha = A$ and B, guiding center y and Landau level n degrees of freedom using a ket $|L, n, \alpha, y\rangle$. This ket, however, will not turn out to be the most convenient basis choice because interlayer terms can shift the guiding center by $\pm\Delta$ with $\Delta = \sqrt{3}k_\theta\ell^2/2$—specifically through processes associated with $T_{2,3}$. This can easily be seen if we compute matrix elements

$$\langle A/B, n, \alpha, y|e^{-i\mathbf{q}_{2,3}\mathbf{x}}|B/A, n, \alpha, y'\rangle \propto \delta_{y,y'\pm\Delta}. \tag{11}$$

By analogy to a tight binding model we can now directly see that the system has a periodicity arising from this restriction to interlayer hopping processes—a magnetic unit cell arises. Now for the resulting Hamiltonian to be diagonalizable for an infinite size system it is important that the moiré unit cell is commensurate with the magnetic unit cell because otherwise one will be dealing with a quasiperiodic system. It is found to be the case when the magnetic flux Φ through a unit cell is such that [63]

$$\Phi = \frac{q}{p}\phi_0, \quad \phi_0 = \frac{hc}{e}, \tag{12}$$

where $p/q \in \mathbb{Q}$ is the rational number relating the flux Φ to the flux quantum ϕ_0, in our case we have chosen units such that $\hbar = c = 1$. It is found that the resulting magnetic moiré

Brillouin zone (MMBZ) is bounded by

$$0 < k_x = \frac{y_0}{\ell^2} < \frac{\Delta}{\ell^2}, \quad 0 < k_y < \frac{2\pi}{q\Delta}, \tag{13}$$

or rewritten to allow a comparison to the nonmagnetic case

$$0 < k_x = \frac{y_0}{\ell^2} < \frac{\sqrt{3}}{2}k_\theta, \quad 0 < k_y < \frac{k_\theta}{2p}. \tag{14}$$

Making use of the periodicity seen in Eq. (11) it is convenient to express the guiding center coordinate as $y = y_0 + (mq + j)\Delta$, where $j \in 0, 1, \ldots, q-1$. A computationally convenient basis is then given by the Fourier transform

$$|L, n, \alpha, j\rangle = \frac{1}{\sqrt{N}} \sum_m e^{ik_y(mq+j)\Delta} |L, n, y_0 + (mq + j)\Delta\rangle, \tag{15}$$

where we dropped the transformed label k_y from the ket on the left side of the equation to simplify the notation because the Hamiltonian will be diagonal in k_y. The intralayer Hamiltonian in this basis is then given as

$$h(\theta/2) = -\omega_c \sum_{L,n,j} (e^{-i\theta_L/2}\sqrt{n+1}|L, n+1, A, j\rangle \times \langle L, n, B, j| + \text{H.c.}). \tag{16}$$

The interlayer Hamiltonian in the same basis can be expressed as

$$\begin{aligned} T(\mathbf{k}) = \sum_{n'n\alpha\beta j} & [T_1 F_{n'n}(\mathbf{z}_1) e^{-ik_x k_\theta \ell^2} e^{-4\pi i \frac{p}{q} j} |2n'\alpha j\rangle\langle 1n\beta j| \\ & + T_2 F_{n'n}(\mathbf{z}_2) e^{ik_y\Delta} e^{\frac{i}{2}k_x k_\theta \ell^2} e^{i\pi \frac{p}{q}(2j-1)} |2n'\alpha, j+1\rangle\langle 1n\beta j| \\ & + T_3 F_{n'n}(\mathbf{z}_3) e^{-ik_y\Delta} e^{\frac{i}{2}k_x k_\theta \ell^2} e^{i\pi \frac{p}{q}(2j+1)} |2n'\alpha j-1\rangle\langle 1n\beta j|], \end{aligned} \tag{17}$$

where $\mathbf{z}_j = \frac{q_{jx}+iq_{jy}}{\sqrt{2}}\ell$, and

$$\begin{aligned} F_{nm}(\mathbf{z}) &= \begin{cases} \tilde{F}_{nm}(\mathbf{z}) & n \geqslant m \\ \tilde{F}^*_{nm}(-\mathbf{z}) & m < n \end{cases}, \\ \tilde{F}_{nm}(\mathbf{z}) &= \sqrt{\frac{m!}{n!}} e^{-\frac{\mathbf{z}^2}{2}} (-z_1 + iz_2)^{n-m} \mathcal{L}_m^{n-m}(\mathbf{z}^2), \end{aligned} \tag{18}$$

where $\mathcal{L}$ is the so-called associated Laguerre polynomial and z_i the components of $\mathbf{z}$.

It is important to expand on one subtlety about the numerical implementation of this Hamiltonian that was mentioned as a brief footnote in Ref. [63]. While the Hamiltonian for the most part is straightforward to implement numerically, one has to be careful about the inclusion of basis states to avoid a spurious degeneracy at low energies. Particularly, let us consider the case where we neglect interlayer couplings. Since we have chosen a model valid near the K point of graphene we have to realize that there is only one zero energy eigenstate per layer and K point. However, if we naively choose our basis states from

$$\{L \in \{t, b\}, \alpha \in \{A, B\}, n \in \{0, \ldots, n_{\max}\}\}, \tag{19}$$

and diagonalize numerically, we find additional spurious states at zero energy. To understand this better we may now recall the analytical expressions for the wave functions of the zero energy Landau level for graphene at the K point. For each layer we find $|n, \pm\rangle = (\pm|n-1\rangle, |n\rangle)$. That is, $n = 0$ only has contributions from sublattice B. Now, we find that there is zero energy states that have contributions from sublattice A, which we can identify as a numerical artifact coming from our choice of basis, which does not break sublattice symmetry. Clearly sublattice symmetry is broken by the solutions and we have to ensure this is enforced in our numerical approach. The way to achieve this is to make a slightly altered choice of basis states that explicitly breaks sublattice symmetry. This choice is given below

$$\{L \in \{t, b\}, \alpha \in \{A, B\}, n \in \{0, \ldots, n_{\max} - \delta_{\alpha,B}\}\}, \tag{20}$$

where the term $\delta_{\alpha,B} = 1$ if the sublattice index α corresponds to sublattice B. That is sublattice B has a smaller Landau level cutoff than sublattice A.

This explicit breaking of sublattice symmetry in the choice of basis states shifts spurious states to high energies, which will be of no consequence for us [63]. We stress that while, in the case of noncoupled layers the spurious low lying levels do not seem to matter in a plot of Landau levels (since the plot does not show degeneracy), this point becomes very important in the presence of interlayer coupling. Indeed, as interlayer couplings get introduced Landau levels split and spurious low energy bands have a devastating effect. Therefore it is of utmost importance to remove the spurious contributions using the approach we have just outlined.

B. Equilibrium properties: interlayer hoppings and the Hofstadter butterfly

Next, we want to study some of the equilibrium properties of this model. First, we recall that it has been noted in Ref. [63] that in the presence of a nonzero magnetic field we find that the Landau levels in TBLG possess a fractal, self-similar structure see Fig. 1(c).

We next want to determine which types of interlayer hopping processes are the most important for the appearance of the Hofstadter butterfly. Therefore, in Fig. 2, we plot the Hofstadter butterfly for different values of the AA-type hopping amplitudes w_0 and AB/BA-type hopping amplitudes w_1.

In Fig. 2(a), we observe that if we set $w_0 = 0$ meV, $w_1 = 110$ meV, which corresponds to the so-called chiral model [95]. For this case, the Hofstadter butterfly at the center of our plot collapses into a zero energy line. The reason that the lowest Landau level collapses can be understood from a perturbative perspective. In essence is due to the fact that the lowest Landau level of graphene lives only on a single sublattice and that the terms proportional to w_1 in $T(\mathbf{r})$ couple between sublattices. Therefore these terms have no effect on the lowest Landau level, which is in stark contrast to other levels, which live on both sublattices. More precisely, treating $V = T(\mathbf{r})$ as a perturbation, the eigen-bi-spinors of the lowest Landau level for $T(\mathbf{r}) = 0$ are $|L_{01}\rangle = (0, |0\rangle, 0, 0)$ or $|L_{02}\rangle = (0, 0, 0, |0\rangle)$. The first correction to the energy because of this can be found as $\langle L_{02}|V|L_{02}\rangle = 0$, of course for $w_0 = 0$. Therefore the lowest Landau level is left unsplit.

To contrast the case $w_0 = 0$ meV we also studied the opposite case of $w_0 = 110$ meV, $w_1 = 0$ in Fig. 2(b).

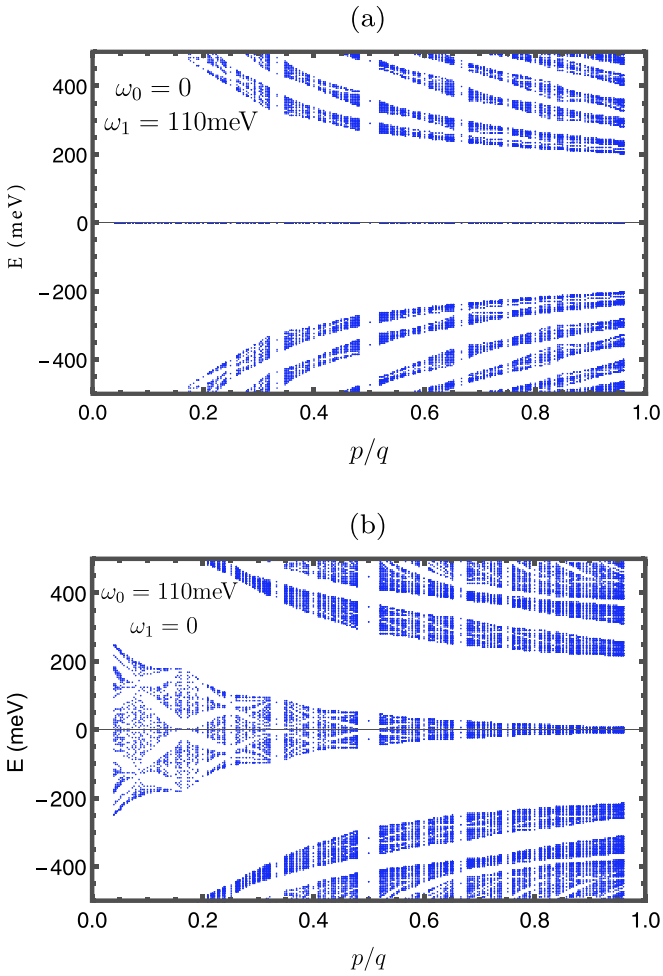

FIG. 2. The Floquet Hofstadter butterfly spectrum as a function of $p/q = \phi_0/\Phi$ in the equilibrium case for different values of the hopping amplitude. (a) $w_0 = 0$, $w_1 = 110$ meV. (b) $w_0 = 110$ meV, $w_1 = 0$ meV. A cutoff for the Landau level index n that was used for the plots is the same as the one suggested in Ref. [63] $n_{\max} \approx 2[\max(a_0\gamma_{\mathrm{RF}}, w_1)/\omega_c]^2$.

Interestingly, we find that in our case it is this term that leads to the splitting of the central Landau level and the appearance of the Hofstadter butterfly. This is in stark contrast to the physics that leads to the appearance of flat bands, where this term is the less important one [95].

We should also note that both reduced models $w_0 = 0$ or $w_1 = 0$ lead to a Hofstadter butterfly that is symmetric with respect to the axis $E = 0$. This is because in these cases—unlike the case where both $w_i \neq 0$—there exist unitary operators C_i with $C_i^2 = 1$ that anticommute with the Hamiltonian. In the case $w_0 = 0$ it is $C_1 = \mathrm{diag}(1, -1, 1, -1)$ and in the case of $w_1 = 0$ it is $C_2 = \mathrm{diag}(1, -1, -1, 1)$. Indeed, from $C_i H\psi_n = -HC_i\psi_n$, one can directly see that each state ψ_n fulfilling $E_n\psi_n = H\psi_n$ has a chiral partner state $C_i\psi_n$ with energy $-E_n$ and hence the spectrum is symmetric [96].

Now the disappearance of the center butterfly in the case $w_0 = 0$ meV, $w_1 = 110$ meV leads to an intuitive understanding of some subtle possible experimental consequences for the measurement of an equilibrium Hofstadter butterfly in a relaxed TBG lattice. Particularly, we may realize that w_0 tunes the strength of the lowest Landau level splitting. This is something that becomes important to recognize because it has been found that w_0-type hoppings become less important as one reduces the twist angle in TBG [97]. This effect, which is due to lattice relaxations, can be captured by a fit of w_0/w_1 for angles $\theta = 0.18^\circ$ to 6° to the data in Fig. 3(c) of Ref. [97] as

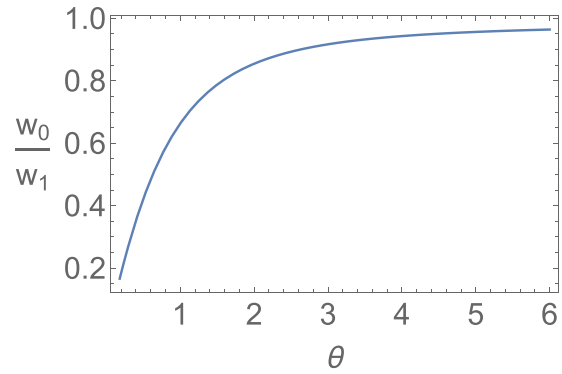

FIG. 3. Plot of the ratio w_0/w_1 as a function of angle (in degree) for the range of its validity.

$$w_0/w_1 \approx \frac{\tan^{-1}\left(\frac{0.0236}{\theta}\right)}{-0.0002 + \frac{0.00001}{\theta^2} + \frac{0.024}{\theta}}. \tag{21}$$

From here we can see that w_0 shrinks at small twist angles like it is shown in Fig. 3 below.

This also means that the lowest Landau level at small twist angles is split slightly less dominantly than in the unrelaxed $w_1 = w_0$ case. Therefore, for a relaxed lattice, one might need a slightly higher (than the $w_0 = w_1$ case) experimental energy resolution to resolve the individual energy levels arising from the lowest Landau level. However, to be fair, this effect is relatively minuscule. For instance at $\theta = 1^\circ$, $w_1 = 110$ meV, and $p/q = 0.05$ the width of the split lowest Landau level is reduced by only 10%. Therefore the additional energy resolution that is needed to resolve the individual levels coming from the lowest Landau level can be estimated at 10% higher than for the case $w_0 = w_1$. Nevertheless, it should be stressed that this effect might potentially be more dominant in other moiré materials.

III. CIRCULARLY POLARIZED LIGHT

In this section, we will turn our attention to the effect that circularly polarized light has on the Hofstadter butterfly in TBLG.

A. Effective Hamiltonian

If perpendicularly incident circularly polarized light (we consider the right-handed or clockwise case) is applied to the graphene layers, at frequency Ω and driving strength A, it enters purely via minimal substitution as [51,58,98]

$$\tilde{k}_x(t) = k_x - A\cos(\Omega t), \quad \tilde{k}_y(t) = k_y - A\sin(\Omega t). \tag{22}$$

Thus we have a time-periodic Hamiltonian satisfying $H(\mathbf{x}, \mathbf{k}, t + 2\pi/\Omega) = H(\mathbf{x}, \mathbf{k}, t)$. It is a well-known fact that some of the physical features of a periodically driven

Hamiltonians can be approximately captured by an effective time independent Hamiltonian [51]. In our case such a description will be advantageous for numerical reasons. Therefore let us briefly recall how to arrive at an effective time independent description and what new physical effects are introduced.

A nonperturbative scheme to find effective time-independent Hamiltonians for a periodically driven system is to transform its Hamiltonian to a rotating frame (RF) $H_R = U^\dagger(t)(H - i\partial_t)U(t)$ via a unitary transformation [51]. If a convenient frame is chosen a subsequent time average generates a Hamiltonian that is more accurate than Hamiltonians found via the usual high frequency approximations such a van Vleck or Floquet-Magnus [45]. With such a properly chosen unitary transformation it was found [51,58] that a highly accurate effective Hamiltonian for TBLG subject to a circularly polarized light is given by

$$H(\mathbf{x}, t) = \begin{pmatrix} h(\theta_1, \mathbf{k}) & \tilde{T}(\mathbf{x}) \\ \tilde{T}^\dagger(\mathbf{x}) & h(\theta_2, \mathbf{k}) \end{pmatrix}. \tag{23}$$

It is important to stress that the derivation from Refs. [51,58] generalizes directly to a case with a magnetic field because the unitary transformations that were used are momentum-independent. In the expression (23) above, we observe that the intralayer Hamiltonians have been modified by light as follows:

$$h(\theta, \mathbf{k}) = v_{\mathrm{RF}} R(\theta)\mathbf{k} \cdot \boldsymbol{\sigma} - \Delta_{\mathrm{RF}}\sigma_3, \tag{24}$$

where again we recall that $R(\theta)$ is a rotation matrix in the layer plane. The Fermi velocity is also modified and becomes

$$v_{\mathrm{RF}} = v_F J_0\left(-\frac{6\gamma}{\Omega} J_1\left(\frac{2Aa_0}{3}\right)\right) J_0\left(\frac{2Aa_0}{3}\right), \tag{25}$$

where J_0 is the zeroth Bessel function of the first kind. Hereby Aa_0 provides a unitless scale of driving strengths. Light also causes the system to acquire a band gap, which is given by

$$\Delta_{\mathrm{RF}} = -\frac{3\gamma}{\sqrt{2}} J_1\left(\frac{2Aa_0}{3}\right) J_1\left(-\frac{6\sqrt{2}\gamma}{\Omega} J_1\left(\frac{2Aa_0}{3}\right)\right). \tag{26}$$

Interlayer tunneling matrices are also modified. If we express $T_j = \sum_i T_{j,i}\sigma_i$, where $T_{j,i}$ are expansion coefficients. Then modified interlayer hopping matrices $\tilde{T}_j$ are given by

$$\tilde{T}_j = \sum_i T_{j,i}\tilde{\sigma}_i, \tag{27}$$

where $\tilde{\sigma}_{1,2} = J_0(\nu)\sigma_{1,2}$ and

$$\begin{aligned} \tilde{\sigma}_0 &= \sigma_0 + (J_0(\sqrt{2}\nu) - 1)\left[\sigma_0 \sin^2\left(\frac{\theta}{2}\right) + \frac{i}{2}\sigma_3 \sin(\theta)\right], \\ \tilde{\sigma}_3 &= \sigma_3 + (J_0(\sqrt{2}\nu) - 1)\left[\sigma_3 \cos^2\left(\frac{\theta}{2}\right) - \frac{i}{2}\sigma_3 \sin(\theta)\right] \end{aligned} \tag{28}$$

with $\nu = (-6\gamma/\Omega)J_1(2Aa_0/3)$.

We may now include the magnetic field in the Landau gauge via minimal substitution and use a convenient basis like in Eq. (15) to express the Hamiltonian in a numerically advantageous form. It is then found that the expressions are almost the same as Eqs. (16) and 17 just with $\omega_c \to \omega_{\mathrm{RF}} = \omega_c v_{\mathrm{RF}}/v_F$ and $T_i \to \tilde{T}_i$, of course with an additional gap term

$$\begin{aligned} H_\Delta = \Delta_{\mathrm{RF}} \sum_{L,n,y} &(|L, n, A, y\rangle\langle L, n, A, y| \\ &- |L, n, B, y\rangle\langle L, n, B, y|), \end{aligned} \tag{29}$$

which we use in our numerical analysis.

B. Numerical results

We will now numerically investigate the effect that circularly polarized light has on the Hofstadter butterfly. For this, we have plotted the Hofstadter butterfly at a fixed driving frequency of $\Omega = 2\gamma$ (chosen to be in the high frequency regime) and various driving strengths, which can be seen in Fig. 4 below We observe that as the driving strength is increased, the asymmetry of the energy levels with respect to $E = 0$ becomes increasingly apparent. Now it is interesting to also consider the cases of either $w_0 = 0$ or $w_1 = 0$ that have a spectrum which in the equilibirum case was symmetric with respect to $E = 0$. In both cases we find that energy levels corresponding to the levels that appear from the split 0-th Landau levels of two decoupled graphene layers (we will call it center branch of the butterfly) move upwards to higher energies as we increase the driving strength Aa_0. This introduces an apparent asymmetry of the spectrum with respect to $E = 0$. The source of this asymmetric behavior is obvious because the chiral symmetry we discussed earlier is broken by the introduction of term Δ_{RF}.

However, interestingly in the case of $w_0 = 0$ and $w_1 \neq 0$, it is found that this asymmetry appears only for the center branch of the butterfly—all other levels, up to numerical accuracy, remain symmetric with respect to $E = 0$. In contrast for the case of $w_1 = 0$ and $w_0 \neq 0$, we find that the complete spectrum becomes asymmetric with respect to $E = 0$ so there seem to be no remnants of a chiral symmetry. Both cases can be seen in Fig. 5.

Finally, it is important to mention that there is an easy way to understand why the center branch of the Hofstadter butterfly moves upward—rather than downward. Particularly, this can be understood from the Landau levels of single graphene layer, which are just split into the branches of our butterfly. Let us first consider two isolated graphene layers. Here, for each layer, the wave function near the K point has the form $\psi_n = (\pm|n-1\rangle, |n\rangle)$. In the case of $n = 0$, one should note that there is only a lower component. For each layer, the gap term Δ_{RF} enters as $-\Delta_{\mathrm{RF}}\sigma_z$. To leading order perturbation theory we can then directly see that this shifts the $n = 0$ Landau level upwards. It may seem surprising that symmetry is broken in this way. We should also point out that while near the K' point the opposite shift $\Delta_{\mathrm{RF}}\sigma_z$ happens, the center band is actually shifted in the same direction as in the case of the K point. This is because for the K' point $\psi_n \to (|n\rangle, \pm|n-1\rangle)$, i.e., the first and second components are flipped, which compensates for the change in the sign of Δ_{RF}. A plot showing this can be found in Appendix. For the remainder of this work, we focus on the physics near the K points of the graphene layers because for our purposes the physics near the K' point does not differ substantially from the physics near the K point.

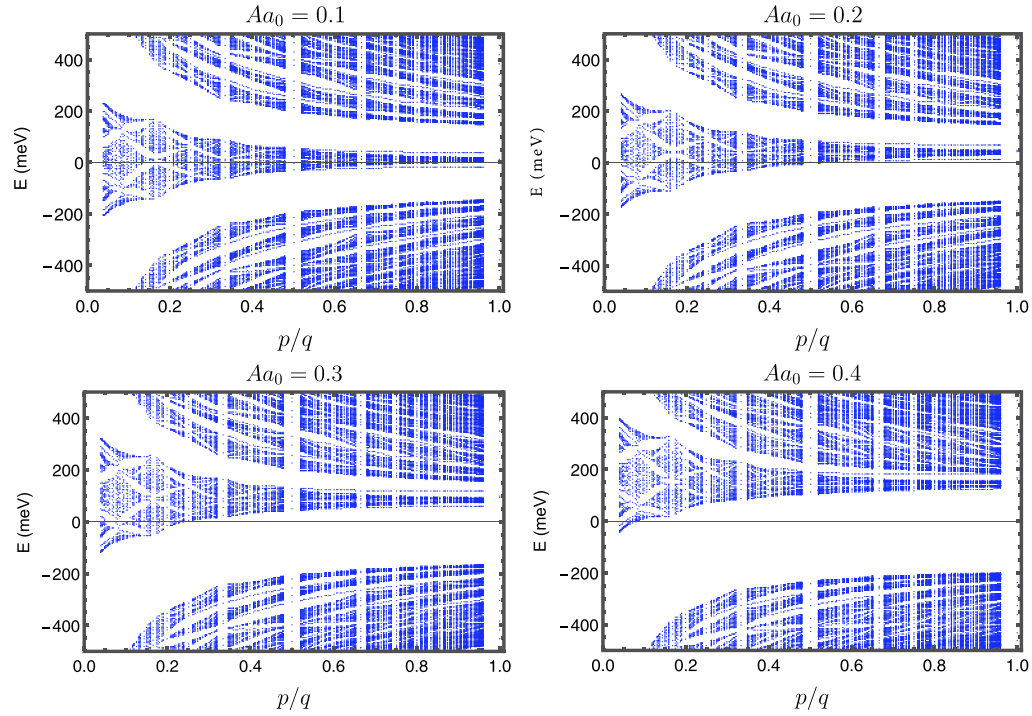

FIG. 4. The Floquet Hofstadter butterfly spectrum as a function of $p/q = \phi_0/\Phi$, subject to right-handed circularly polarized light with driving frequency fixed at $\Omega = 2\gamma$. The representative driving strengths are chosen as $Aa_0 = 0.1$, $Aa_0 = 0.2$, $Aa_0 = 0.3$, and $Aa_0 = 0.4$. The parameters used are $\gamma = 2364$ meV, $w_0 = 0.9w_1$, $w_1 = 110$ meV, and $\theta = 2^\circ$. The Landau level cutoff that was used for the plots is the same as the one suggested in Ref. [63] $n_{\max} \approx 2[\max(a_0\gamma_{\mathrm{RF}}, w_1)/\omega_c]^2$

Lastly, we may consider the question on how to obtain a center band that is shifted downward, rather than upward. This can be answered quite easily via left handed circularly polarized light, which can be seen in Fig. 6.

We see that the center Landau level is shifted downward just as we wanted. This can be understood quite easily. Specifically, to leading order in Floquet theory it is found easily that the main effect of the change from right-handed to left-handed circularly polarized light is the replacement $\Delta_{\mathrm{RF}} \to -\Delta_{\mathrm{RF}}$. That is, the lowest Landau level is shifted downward rather than up like in the case of right-handed circularly polarized light.

IV. WAVEGUIDE LIGHT

After our discussion of circularly polarized light, in this next section we will focus on the effects due to a second type of light, a linearly polarized light emanating from a waveguide.

A. Theoretical approach

The second type of light that will be considered is longitudinal light coming from a waveguide. Here, the boundary conditions of a waveguide allow for light with longitudinal components $\mathbf{A} = \mathrm{Re}(e^{ik_z z - i\Omega t})\hat{z}$ to exist, which is not possible in a vacuum—this expression is valid in a carefully chosen spatial region (more details can be found in the Appendix [60] or most standard references on electromagnetism such as Ref. [99]). The effect of this light can be included within the tight binding model via a Peirls substitution $t_{ij} \to t_{ij}\exp(-\int_{\mathbf{r}_i}^{\mathbf{r}_j} d\mathbf{l}\mathbf{A})$. In the continuum Hamiltonian interlayer hopping terms correspond to w_i, which is why the $w_i \to w_i \exp(-\int_{\mathbf{r}_i}^{\mathbf{r}_j} d\mathbf{l}\mathbf{A})$. To leading order in the high frequency regime of our continuum model (that is the average of the Hamiltonian over one period) this effect can be captured if we replace interlayer couplings as given below

$$w_0 \to w_0 J_0(Aa_{\mathrm{AA}}), \quad w_1 \to w_1 J_0(Aa_{\mathrm{AB}}). \tag{30}$$

More details on the derivation can be found in Ref. [60]. We note that in Ref. [60] it is also found that this lowest order approximation captures most of the features of a more detailed treatment that uses an extended space approach. We therefore restrict our attention to this case. Hereby, $a_{\mathrm{AA}} = 0.36$ nm and $a_{\mathrm{AB}} = 0.34$ nm are interlayer distances in AA and AB regions of TBG. We should note that with the interlayer spacing we made the assumption that AA and AB stacked regions are well pronounced enough to have the corresponding lattice spacing. This is a simplification of the model that becomes well justified in the case of very small twist angles where AB stacked regions become increasingly pronounced due to lattice relaxation effects.

B. Numerical results

We will now discuss the effect of the waveguide light on the Hofstadter butterfly via numeric results. Since the effect that waveguide light has on the Hofstadter butterfly does not differ considerably between the K and K' points, we chose to only consider the case of the K point.

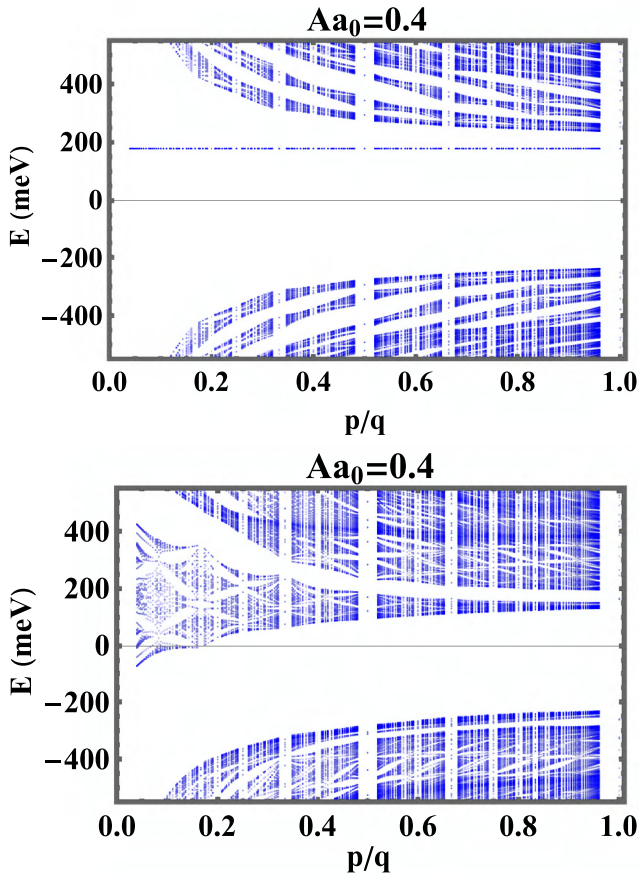

FIG. 5. The Floquet Hofstadter butterfly spectrum as a function of $p/q = \phi_0/\Phi$, subject to right-handed circularly polarized light with driving frequency fixed at $\Omega = 2\gamma$, where $\gamma = 2364$ meV. A representative driving strength is chosen as $Aa_0 = 0.4$ and the angle was set as $\theta = 2^\circ$. The top figure corresponds to the case $w_0 = 0$, $w_1 = 110$ meV, and bottom figure $w_0 = 110$, $w_1 = 0$ meV. The Landau level cutoff that was used for the plots is the same as the one suggested in Ref. [63] $n_{\max} \approx 2[\max(a_0\gamma_{\mathrm{RF}}, w_1)/\omega_c]^2$

Here, we consider a range of different values for our unitless driving strength Aa_{AA}. Note that

$$Aa_{\mathrm{AB}} = \frac{a_{\mathrm{AB}}}{a_{\mathrm{AA}}} Aa_{\mathrm{AA}}. \tag{31}$$

We consider different values for the driving strength in the range $Aa_{\mathrm{AA}} = 0.2$ to 4 in Fig. 7 below. We find that the level splitting of the individual Landau levels first decreases as we increase Aa_{AA} and then eventually increases again. This can be explained very easily using the fact that w_0 and w_1 set the scale for the size of level splitting, which in our case are modulated by Bessel functions J_0. This observation of course allows us to go one step further to find that the two chiral models either $w_1 = 0$ or $w_0 = 0$ can be realized via this form of light. Particularly, w_0 is effectively set to zero if $Aa_{\mathrm{AA}} = j_{0,n}$ is the nth zero of the Bessel function $J_0(x)$. Similarly w_1 is effectively set to zero if $Aa_{\mathrm{AA}} = (a_{\mathrm{AA}}/a_{\mathrm{AB}})j_{0,n}$. At these points the mirror symmetry of the spectrum with respect to $E = 0$ is restored.

We should stress regarding the appropriateness of the approximation in Eq. (30). When the band structure resulting from this approximation was compared to band structures resulting from a full extended space treatment of the time dependent problem such as in Ref. [60] it was found that even at driving strengths as high as $\eta = Aa_{\mathrm{AA}} = 4$ the approximation yielded results that were almost indistinguishable from the exact extended space treatment.

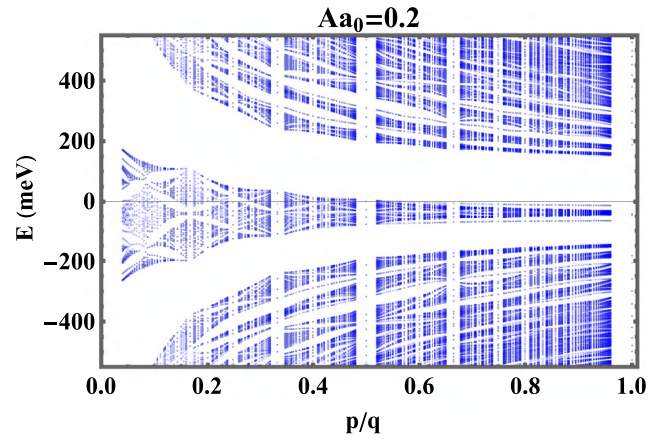

FIG. 6. The Floquet Hofstadter butterfly spectrum as a function of $p/q = \phi_0/\Phi$, subject to left-handed circularly polarized light with driving frequency fixed at $\Omega = 2\gamma$. A representative driving strength was as $Aa_0 = 0.2$. The parameters used are, $\gamma = 2364$ meV, $w_0 = 0.9w_1$, $w_1 = 110$ meV, and $\theta = 2^\circ$. The Landau level cutoff that was used for the plots is the same as the one suggested in Ref. [63] $n_{\max} \approx 2[\max(a_0\gamma_{\mathrm{RF}}, w_1)/\omega_c]^2$

Last, but not the least, regarding the potential experimental realizability of such large driving strengths. We can recall that (reintroducing units) $\eta = \frac{eEa_{\mathrm{AA}}}{\hbar\Omega}$ (see Ref. [60]). Here, for driving frequencies in the high frequency regime $\hbar\Omega > 2.7$ eV and electric field strengths up to $E < 15$ meV/cm, $\eta < 0.2$ is rather limited. Here, the high frequency assumption $\hbar\Omega > 2.7$ eV is our main limiting factor. However, Landau levels are flat and therefore one can find regimes of p/q and θ where $\hbar\Omega < 100$ meV is a high frequency regime for the center part of the Hofstadter butterfly [see, e.g., Fig. 1(c) to identify such a regime visually—being careful that for the high frequency regime the driving strength also needs to be smaller than the gap size]. Therefore our high-frequency approximation can be justified with certain restrictions while values of $\eta > 4$ are achievable experimentally. Therefore both chiral limits of TBLG should be achievable experimentally by employing waveguide light.

Lastly, we consider the case where one starts from one of the chiral limits $w_0 = 0$ or $w_1 = 0$. Here, we find that this form of light does not lead to chiral symmetry breaking, in contrast to the circularly polarized light case.

V. SUMMARY AND CONCLUSION

We have studied the Floquet Hofstadter butterfly spectrum in TBLG subject to a uniform perpendicular magnetic field both in the equilibrium case and in the presence of different forms of light. We have focused on the cases of circularly polarized light and waveguide linearly polarized light. For the equilibrium case, we have identified two separate chiral limits and found that one of them—$w_0 \neq 0$ and $w_1 = 0$—includes most of the butterfly physics.

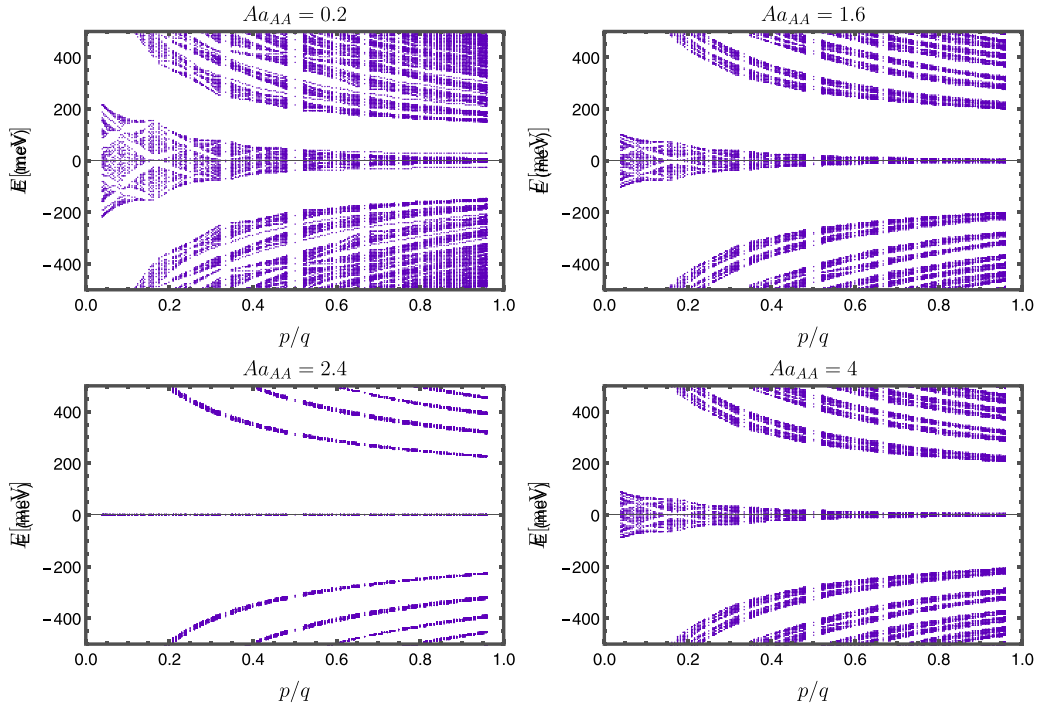

FIG. 7. The Floquet Hofstadter butterfly spectrum as a function of $p/q = \phi_0/\Phi$, subject to waveguide light. The representative driving strengths are chosen from $Aa_{\mathrm{AA}} = 0.2$ to $Aa_{\mathrm{AA}} = 4$. The parameters used are $\gamma = 2364$ meV and $\theta = 2^\circ$.

In the case of circularly polarized light, we have found that the main effect is the creation of a gap term that breaks chiral symmetry. This causes the Hofstadter butterfly to deform such that levels are visibly and based on numerical grounds less mirror symmetric with respect to $E = 0$. In the case of waveguide light we have found that it does not break chiral symmetries if they are present from the start. Interestingly, field driving strength can be selected to achieve both of TBLG's chiral limits. That is, we have found a way to design an experimentally accessible regime that allows the realization of the two chiral limits of TBLG.

ACKNOWLEDGMENTS

H.B. and M.V. gratefully acknowledge the support provided by the Deanship of Research Oversight and Coordination (DROC) at King Fahd University of Petroleum & Minerals (KFUPM) for funding this work through start up Project No. SR211001.

APPENDIX: DISCUSSION OF THE K' POINT

For the reader's convenience, we have also included in this section a brief discussion of the K' point. First we note that the Hamiltonian in the Landau level basis can be obtained if we make the following replacements, which are equivalent to the replacements that were mentioned in the main text.

$$h(\theta/2) \to \omega_c \sum_{L,n,j} (e^{-i\theta/2}\sqrt{n+1}|L, n+1, B, j\rangle\langle L, n, A, j| + \mathrm{H.c.}),$$
$$\mathbf{q}_i \to -\mathbf{q}_i; \quad \zeta \to \zeta^*; \quad \Delta_{\mathrm{RF}} \to -\Delta_{\mathrm{RF}}; \quad \theta \to -\theta. \tag{A1}$$

We stress that one has to be careful about the order of these replacements and apply them in the listed order. Another subtle point one has to be mindful about is that one has to ensure the correct type of sublattice symmetry breaking through the choice of basis set—the lowest Landau level state at each K or K' point does not have this symmetry. Therefore, to ensure a numerical error that happens only at large energies one had to introduce basis sets for A and B sublattices that are altered from the main text but serve the same purpose, which is to remove spurious low energy states. Recall that

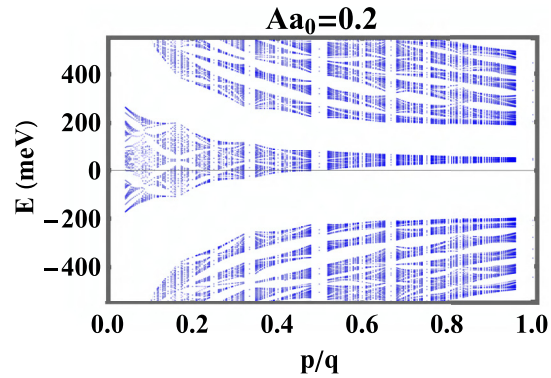

FIG. 8. The Floquet Hofstadter butterfly spectrum as a function of $p/q = \phi_0/\Phi$, subject to right-handed circularly polarized light with driving frequency fixed at $\Omega = 2\gamma$. A representative driving strength was chosen as $Aa_0 = 0.2$. The parameters used are, $\gamma = 2364$ meV, $w_0 = 0.9w_1$, $w_1 = 110$ meV, and $\theta = 2^\circ$. The Landau level cutoff that was used for the plots is the same as the one suggested in Ref. [63] $n_{\max} \approx 2[\max(a_0\gamma_{\mathrm{RF}}, w_1)/\omega_c]^2$. The plot is valid near the K' point. The top right of Fig. 8 is a comparable figure for the K point.

$(\pm|n-1\rangle, |n\rangle) \rightarrow (\pm|n\rangle, |n-1\rangle)$. Particularly our choice of basis has to be according to

$$\{L \in \{t, b\}, \alpha \in \{A, B\}, n \in \{0, \ldots, n_{\max} - \delta_{\alpha,A}\}\}, \quad \text{(A2)}$$

where L is the layer degree of freedom, α the sublattice and n the Landau level index. The term $\delta_{\alpha,A}$ ensures that the Landau level index is truncated earlier for sublattice A.

With these changes to the Hamiltonian we were able to generate plots that are valid near the K' point. The presumably most interesting situation occurs in the case of circularly polarized light with a plot in Fig. 8 given below

We see that even for this case there is no major physics that differs fundamentally from the physics near the K point, this validates our decision to consider only the K point in our main text.

[1] K. S. Novoselov, A. K. Geim, S. V. Morozov, D. Jiang, Y. Zhang, S. V. Dubonos, I. V. Grigorieva, and A. A. Firsov, Electric field effect in atomically thin carbon films, Science **306**, 666 (2004).

[2] A. H. Castro Neto, F. Guinea, N. M. R. Peres, K. S. Novoselov, and A. K. Geim, The electronic properties of graphene, Rev. Mod. Phys. **81**, 109 (2019).

[3] W.-X. Wang, L.-J. Yin, J.-B. Qiao, T. Cai, S.-Y. Li, R.-F. Dou, J.-C. Nie, X. Wu, and L. He, Atomic resolution imaging of the two-component Dirac-Landau levels in a gapped graphene monolayer, Phys. Rev. B **92**, 165420 (2015).

[4] P. San-Jose, A. Gutiérrez-Rubio, M. Sturla, and F. Guinea, Spontaneous strains and gap in graphene on boron nitride, Phys. Rev. B **90**, 075428 (2014).

[5] M. Kindermann, B. Uchoa, and D. L. Miller, Zero-energy modes and gate-tunable gap in graphene on hexagonal boron nitride, Phys. Rev. B **86**, 115415 (2012).

[6] M. Zarenia, O. Leenaerts, B. Partoens, and F. M. Peeters, Substrate-induced chiral states in graphene, Phys. Rev. B **86**, 085451 (2012).

[7] S. Y. Zhou, D. A. Siegel, A. V. Fedorov, and A. Lanzara, Metal to Insulator Transition in Epitaxial Graphene Induced by Molecular Doping, Phys. Rev. Lett. **101**, 086402 (2008).

[8] R. N. Costa Filho, G. A. Farias, and F. M. Peeters, Graphene ribbons with a line of impurities: Opening of a gap, Phys. Rev. B **76**, 193409 (2007).

[9] Gerardo G. Naumis, E. Aguilar-Méndez, and A. Espinosa-Champo, Atomic resolution imaging of the two-component Dirac-Landau levels in a gapped graphene monolayer, Phys. Rev. B **103**, 245418 (2021).

[10] B. Van Duppen and F. M. Peeters, Four-band tunneling in bilayer graphene, Phys. Rev. B **87**, 205427 (2013).

[11] M. Van der Donck, F. M. Peeters, and B. Van Duppen, Transport properties of bilayer graphene in a strong in-plane magnetic field, Phys. Rev. B **93**, 115423 (2016).

[12] M. Barbier, P. Vasilopoulos, and F. M. Peeters, Kronig-Penney model on bilayer graphene: Spectrum and transmission periodic in the strength of the barriers, Phys. Rev. B **82**, 235408.

[13] I. Snyman and C. W. J. Beenakker, Ballistic transmission through a graphene bilayer, Phys. Rev. B **75**, 045322 (2007).

[14] E. McCann and V. I. Falko, Landau-Level Degeneracy and Quantum Hall Effect in a Graphite Bilayer, Phys. Rev. Lett. **96**, 086805 (2006).

[15] A. Rozhkov, A. Sboychakov, A. Rakhmanov, and F. Nori, Electronic properties of graphene-based bilayer systems, Phys. Rep. **648**, 1 (2016).

[16] T. Ohta, A. Bostwick, T. Seyller, K. Horn, and E. Rotenberg, Controlling the electronic structure of bilayer graphene, Science **313**, 951 (2006).

[17] N. Benlakhouy, A. El Mouhafid, and A. Jellal, Transport properties in gapped bilayer graphene, Phys. E **134**, 114835 (2021).

[18] C.-W. Chiu, S.-C. Chen, Y.-C. Huang, F.-L. Shyu, and M.-F. Lin, Critical optical properties of AA-stacked multilayer graphenes, Appl. Phys. Lett. **103**, 041907 (2013).

[19] Y. Zahidi, I. Redouani, and A. Jellal, GoosHänchen shifts in AA-stacked bilayer graphene superlattices, Phys. E **81**, 259 (2016).

[20] Y. Cao, V. Fatemi, S. Fang, K. Watanabe, T. Taniguchi, E. Kaxiras, and P. Jarillo-Herrero, Unconventional superconductivity in magic-angle graphene superlattices, Nature (London) **556**, 43 (2018).

[21] F. J. Culchac, R. R. Del Grande, R. B. Capaz, L. Chico, and E. S. Morell, Flat bands and gaps in twisted double bilayer graphene, Nanoscale **12**, 5014 (2020).

[22] Y. Cao, D. Rodan-Legrain, O. Rubies-Bigorda, J. M. Park, K. Watanabe, T. Taniguchi, and P. Jarillo-Herrero, Tunable correlated states and spin-polarized phases in twisted bilayerbilayer graphene, Nature (London) **583**, 215 (2020).

[23] C. Shen, Y. Chu, Q. Wu, N. Li, S. Wang, Y. Zhao, J. Tang, J. Liu, J. Tian, K. Watanabe, T. Taniguchi, R. Yang, Z. Y. Meng, D. Shi, O. V. Yazyev, and G. Zhang, Correlated states in twisted double bilayer graphene, Nat. Phys. **16**, 520 (2020).

[24] X. Liu, Z. Hao, E. Khalaf, J. Y. Lee, Y. Ronen, H. Yoo, D. Haei Najafabadi, K. Watanabe, T. Taniguchi, A. Vish-wanath, and P. Kim, Tunable spin-polarized correlated states in twisted double bilayer graphene, Nature (London) **583**, 221 (2020).

[25] Jong Yeon Yeon Lee, E. Khalaf, S. Liu, X. Liu, Z. Hao, P. Kim, and A. Vishwanath, Theory of correlated insulating behaviour and spin-triplet superconductivity in twisted double bilayer graphene, Nat. Commun. **10**, 5333 (2019).

[26] A. Kerelsky, C. Rubio-Verdú, L. Xian, D. M. Kennes, D. Halbertal, N. Finney, L. Song, S. Turkel, L. Wang, K. Watanabe, T. Taniguchi, J. Hone, C. Dean, D. Basov, A. Rubio, and A. N. Pasupathy, Moiré-less correlations in abca graphene, Proc. Nat. Acad. Sci. **118**, e2017366118 (2021).

[27] C. Rubio-Verdú, S. Turkel, L. Song, L. Klebl, R. Samaj-dar, M. S. Scheurer, J. W. F. Venderbos, K. Watanabe, T. Taniguchi, H. Ochoa, L. Xian, D. Kennes, R. M. Fer-nandes, A. Rubio, and A. N. Pasupathy, Moiré nematic phase in twisted double bilayer graphene, Nat. Phys. **18**, 196 (2022).

[28] D. Halbertal, N. R. Finney, S. S. Sunku, A. Kerelsky, C. Rubio-Verdú, S. Shabani, L. Xian, S. Carr, S. Chen, C. Zhang, L. Wang, D. Gonzalez-Acevedo, A. S. McLeod, D. Rhodes, K. Watanabe, T. Taniguchi, E. Kaxiras, C. R. Dean, J. C. Hone, A. N. Pasupathy *et al.* Moiré metrology of energy land-scapes in van der Waals heterostructures, Nat. Commun. **12**, 242 (2021).

[29] M. Christos, S. Sachdev, and M. S. Scheurer, Correlated insulators, semimetals, and superconductivity in twisted trilayer graphene, arXiv:2106.02063, (2021).

[30] D. Wong, K. P. Nuckolls, M. Oh, B. Lian, Y. Xie, S. Jeon, K. Watanabe, T. Taniguchi, B. A. Bernevig, and A. Yaz-dani, Cascade of electronic transitions in magic-angle twisted bilayer graphene, Nature (London) **582**, 198 (2020).

[31] X. Lu, P. Stepanov, W. Yang, M. Xie, M. A. Aamir, I. Das, C. Urgell, K. Watanabe, T. Taniguchi, G. Zhang, A. Bachtold, A. H. MacDonald, and D. K. Efetov, Superconductors, orbital magnets and correlated states in magic-angle bilayer graphene, Nature (London) **574**, 653 (2019).

[32] A. L. Sharpe, E. J. Fox, A. W. Barnard, J. Finney, K. Watanabe, T. Taniguchi, M. A. Kastner, and D. Goldhaber-Gordon, Emergent ferromagnetism near three-quarters filling in twisted bilayer graphene, Science **365**, 605 (2019).

[33] K. Seo, V. N. Kotov, and B. Uchoa, Ferromagnetic Mott state in Twisted Graphene Bilayers at the Magic Angle, Phys. Rev. Lett. **122**, 246402 (2019).

[34] J. Hass, F. Varchon, J. E. Millan-Otoya, M. Sprinkle, N. Sharma, W. A. deHeer, C. Berger, P. N. First, L. Magaud, and E. H. Conrad, Why Multilayer Graphene on 4H-SiC(000$\bar{1}$Â) Behaves Like a Single Sheet of Graphene, Phys. Rev. Lett. **100**, 125504 (2008).

[35] I. Brihuega, P. Mallet, H. González-Herrero, G. Trambly de Laissardière, M. M. Ugeda, L. Magaud, J. M. Gómez-Rodríguez, F. Ynduráin, and J.-Y. Veuillen, Unraveling the Intrinsic and Robust Nature of van Hove Singularities in Twisted Bilayer Graphene by Scanning Tunneling Microscopy and Theoretical Analysis, Phys. Rev. Lett. **109**, 196802 (2012).

[36] L. Meng, Y. Zhang, W. Yan, L. Feng, L. He, R.-F. Dou, and J.-C. Nie, Single-layer behavior and slow carrier density dynamic of twisted graphene bilayer, Appl. Phys. Lett. **100**, 091601 (2012).

[37] A. Luican, G. Li, A. Reina, J. Kong, R. R. Nair, K. S. Novoselov, A. K. Geim, and E. Y. Andrei, Single-Layer Behavior and Its Breakdown in Twisted Graphene Layers, Phys. Rev. Lett. **106**, 126802 (2011).

[38] W. Yan, M. Liu, R.-F. Dou, L. Meng, L. Feng, Z.-D. Chu, Y. Zhang, Z. Liu, J.-C. Nie, and L. He, Angle-Dependent van Hove Singularities in a Slightly Twisted Graphene Bilayer, Phys. Rev. Lett. **109**, 126801 (2012).

[39] G. Li, A. Luican, J. M. B. Lopes dos Santos, A. H. Castro Neto, A. Reina, J. Kong, and E. Y. Andrei, Observation of Van Hove singularities in twisted graphene layers, Nat. Phys. **6**, 109 (2010).

[40] E. Cisternas and J. D. Correa, Theoretical reproduction of superstructures revealed by STM on bilayer graphene, Chem. Phys. **409**, 74 (2012).

[41] T. Oka and S. Kitamura, Floquet engineering of quantum materials, Annu. Rev. Condens. Matter Phys. **10**, 387 (2019).

[42] T. Oka and H. Aoki, Photovoltaic hall effect in graphene, Phys. Rev. B **79**, 081406(R) (2009).

[43] M. Luo, Tuning of a bilayer graphene heterostructure by horizontally incident circular polarized light, Phys. Rev. B **103**, 195422 (2021).

[44] O. V. Kibis, S. Morina, K. Dini, and I. A. Shelykh, Magneto-electronic properties of graphene dressed by a high-frequency field, Phys. Rev. B **93**, 115420 (2016).

[45] M. Rodriguez-Vega, M. Vogl, and G. A. Fiete, Low-frequency and Moiré Floquet engineering: Areview, Ann. Phys. **435** 168434 (2021).

[46] D. A. Abanin, W. De Roeck, W. W. Ho, and F. m. c. Huveneers, Effective Hamiltonians, prethermalization, and slow energy absorption in periodically driven many-body systems, Phys. Rev. B **95**, 014112 (2017).

[47] A. P. Itin and M. I. Katsnelson, Effective Hamiltonians for Rapidly Driven Many-Body Lattice Systems: Induced Exchange Interactions and Density-Dependent Hoppings, Phys. Rev. Lett. **115**, 075301 (2015).

[48] T. Mikami, S. Kitamura, K. Yasuda, N. Tsuji, T. Oka, and H. Aoki, Brillouin-Wigner theory for high-frequency expansion in periodically driven systems: Application to Floquet topological insulators, Phys. Rev. B **93**, 144307 (2016).

[49] P. Mohan, R. Saxena, A. Kundu, and S. Rao, Brillouin-Wigner theory for Floquet topological phase transitions in spin-orbit-coupled materials, Phys. Rev. B **94**, 235419 (2016).

[50] M. Vogl, P. Laurell, A. D. Barr, and G. A. Fiete, Analog of hamilton-jacobi theory for the time-evolution operator, Phys. Rev. A **100**, 012132 (2019).

[51] M. Vogl, M. Rodriguez-Vega, G. A. Fiete, Effective Floquet Hamiltonians for periodically driven twisted bilayer graphene, Phys. Rev. B **101**, 235411 (2020).

[52] M. Vogl, P. Laurell, A. D. Barr, and G. A. Fiete, Flow Equation Approach to Periodically Driven Quantum Systems, Phys. Rev. X **9**, 021037 (2019).

[53] M. Rodriguez-Vega, M. Lentz, and B. Seradjeh, Floquet perturbation theory: Formalism and application to low-frequency limit, New J. Phys. **20**, 093022 (2018).

[54] M. Rodriguez-Vega and B. Seradjeh, Universal Fluctuations of Floquet Topological Invariants at Low Frequencies, Phys. Rev. Lett. **121**, 036402 (2018).

[55] D. M. Kennes, N. Müller, M. Pletyukhov, C. Weber, C. Bruder, F. Hassler, J. Klinovaja, D. Loss, and H. Schoeller, Chiral one-dimensional floquet topological insulators beyond the rotating wave approximation, Phys. Rev. B **100**, 041103(R) (2019).

[56] Z.-Z. Li, C.-H. Lam, and J. Q. You, Floquet engineering of long-range p-wave superconductivity: Beyond the high-frequency limit, Phys. Rev. B **96**, 155438 (2017).

[57] N. Müller, D. M. Kennes, J. Klinovaja, D. Loss, and H. Schoeller, Electronic transport in one-dimensional floquet topological insulators via topological and nontopological edge states, Phys. Rev. B **101**, 155417 (2020).

[58] I. A. Assi, J. P. F. LeBlanc, M. Rodriguez-Vega, H. Bahlouli, and M. Vogl, Floquet engineering and non-equilibrium topological maps in twisted trilayer graphene, Phys. Rev. B **104**, 195429 (2021).

[59] G. E. Topp, G. Jotzu, J. W. McIver, L. Xian, A. Rubio, and M. A. Sentef, Topological floquet engineering of twisted bilayer graphene, Phys. Rev. Research **1**, 023031 (2019).

[60] M. Vogl, M. Rodriguez-Vega, G. A. Fiete, Floquet engineering of interlayer couplings: Tuning the magic angle of twisted bilayer graphene at the exit of a waveguide, Phys. Rev. B **101**, 241408(R) (2020).

[61] M. Lu, J. Zeng, H. Liu, J.-H. Gao, and X. C. Xie, Valley-selective floquet chern flat bands in twisted multilayer graphene, Phys. Rev. B **103**, 195146 (2021).

[62] M. Rodriguez-Vega, M. Vogl, and G. A. Fiete, Floquet engineering of twisted double bilayer graphene, Phys. Rev. Research **2**, 033494 (2020).

[63] R. Bistritzer and A. H. MacDonald, moiré butterflies in twisted bilayer graphene, Phys. Rev. B **84**, 035440 (2011).

[64] J. Herzog-Arbeitman, A. Chew, D. K. Efetov, and B. A. Bernevig, Reentrant correlated insulators in twisted bilayer graphene at 25T (2π flux), arXiv:2111.11434.

[65] I. Das, C. Shen, A. Jaoui, J. Herzog-Arbeitman, A. Chew, C.-W. Cho, T. Taniguchi, K. Watanabe, B. Piot, B. A. Bernevig, and D. K. Efetov, Observation of re-entrant correlated insulators and interaction driven Fermi surface reconstructions at one magnetic flux quantum per moiré unit cell in magic-angle twisted bilayer graphene, arXiv:2111.11341.

[66] B. Andrews and A. Soluyanov, Fractional quantum Hall states for moiré superstructures in the Hofstadter regime, Phys. Rev. B **101**, 235312 (2020).

[67] K. Hejazi, C. Liu, and L. Balents, Landau levels in twisted bilayer graphene and semiclassical orbits, Phys. Rev. B **100**, 035115 (2019).

[68] D. R. Hofstadter, Energy levels and wave functions of Bloch electrons in rational and irrational magnetic fields, Phys. Rev. B **14**, 2239 (1976).

[69] B. Hunt, J. D. Sanchez-Yamagishi, A. F. Young, M. Yankowitz, B. J. LeRoy, K. Watanabe, T. Taniguchi, P. Moon, M. Koshino, P. Jarillo-Herrero, and R. C. Ashoori, Massive dirac fermions and hofstadter butterfly in a van der waals heterostructure, Science **340**, 1427 (2013).

[70] L. A. Ponomarenko, R. V. Gorbachev, G. L. Yu, D. C. Elias, R. Jalil, A. A. Patel, A. Mishchenko, A. S. Mayorov, C. R. Woods, J. R. Wallbank, M. Mucha-Kruczynski, B. A. Piot, M. Potemski, I. V. Grigorieva, K. S. Novoselov, F. Guinea, V. I. Falko, and A. K. Geim, Cloning of Dirac fermions in graphene superlattices, Nature (London) **497**, 594 (2013).

[71] C. R. Dean, L. Wang, P. Maher, C. Forsythe, F. Ghahari, Y. Gao, J. Katoch, M. Ishigami, P. Moon, M. Koshino *et al.*, Hofstadters butterfly and the fractal quantum Hall effect in moiré superlattices, Nature (London) **497**, 598 (2013).

[72] G.-Y. Oh, Energy spectrum of a triangular lattice in a uniform magnetic field: Effect of next-nearest-neighbor hopping, J. Korean Phys. Soc. **37**, 534 (2000).

[73] G.-Y. Oh, Energy spectrum of a honeycomb lattice under nonuniform magnetic fields, J. Korean Phys. Soc. **49**, 672 (2006).

[74] L. Du, Q. Chen, A. D. Barr, A. R. Barr, and G. A. Fiete, Floquet Hofstadter butterfly on the kagome and triangular lattices, Phys. Rev. B **98**, 245145 (2018).

[75] R. Bistritzer and A. H. MacDonald, moiré bands in twisted double-layer graphene, Proc. Natl. Acad. Sci. USA **108**, 12233 (2011).

[76] Ya-Hui Zhang, H. C. Po, and T. Senthil, Landau level degeneracy in twisted bilayer graphene: Role of symmetry breaking, Phys. Rev. B **100**, 125104 (2019).

[77] J. Wang, A. S. Mouritzen, and J. Gong, Quantum control of ultra-cold atoms: Uncovering a novel connection between two paradigms of quantum nonlinear dynamics, J. Mod. Opt. **56**, 722 (2009).

[78] W. Lawton, A. S. Mouritzen, J. Wang, and J. Gong, Spectral relationships between kicked Harper and on-resonance double kicked rotor operators, J. Math. Phys. **50**, 032103 (2009).

[79] H. Wang, D. Y. H. Ho, W. Lawton, J. Wang, and J. Gong, Kicked-Harper model versus on-resonance double-kicked rotor model: From spectral difference to topological equivalence, Phys. Rev. E **88**, 052920 (2013).

[80] M. Lababidi, I. I. Satija, and E. Zhao, Counter-propagating Edge Modes and Topological Phases of a Kicked Quantum Hall System, Phys. Rev. Lett. **112**, 026805 (2014).

[81] Z. Zhou, I. I. Satija, and E. Zhao, Floquet edge states in a harmonically driven integer quantum Hall system, Phys. Rev. B **90**, 205108 (2014).

[82] K.-H. Ding, L.-K. Lim, G. Su, and Z.-Y. Weng, Quantum Hall effect in ac driven graphene: From the half-integer to the integer case, Phys. Rev. B **97**, 035123 (2018).

[83] M. Wackerl and J. Schliemann, Driven hofstadter butterflies and related topological invariants, Phys. Rev. B **100**, 165411 (2019).

[84] S. H. Kooi, A. Quelle, W. Beugeling, and C. Morais Smith, Genesis of the Floquet Hofstadter butterfly, Phys. Rev. B **98**, 115124 (2018).

[85] P. Moon and M. Koshino, Optical properties of the Hofstadter butterfly in the moiré superlattice, Phys. Rev. B **88**, 241412(R) (2013).

[86] J. A. Crosse and P. Moon, Faraday rotations, ellipticity and circular dichroism in the magneto-optical spectrum of moiré superlattices, Chin. Phys. B **30**, 077803 (2021).

[87] F. Wu, A. H. MacDonald, and I. Martin, Theory of Phonon-Mediated Superconductivity in Twisted Bilayer Graphene, Phys. Rev. Lett. **121**, 257001 (2018).

[88] F. Rost, R. Gupta, M. Fleischmann, D. Weckbecker, N. Ray, J. Olivares, M. Vogl, S. Sharma, O. Pankratov, and S. Shallcross, Nonperturbative theory of effective Hamiltonians for deformations in two-dimensional materials: Moiré systems and dislocations, Phys. Rev. B **100**, 035101 (2019).

[89] M. Fleischmann, R. Gupta, F. WullschlÃ¤ger, S. Theil, D. Weckbecker, V. Meded, S. Sharma, B. Meyer, and S. Shallcross, Perfect and controllable nesting in minimally twisted bilayer graphene, Nano Lett. **20**, 971 (2020).

[90] M. Xie and A. H. MacDonald, Nature of the Correlated Insulator States in Twisted Bilayer Graphen, Phys. Rev. Lett. **124**, 097601 (2020).

[91] K. Hejazi, C. Liu, H. Shapourian, X. Chen, and L. Balents, Multiple topological transitions in twisted bilayer graphene near the first magic angle, Phys. Rev. B **99**, 035111 (2019).

[92] M. Fleischmann, R. Gupta, S. Sharma, and S. Shallcross, Moiré quantum well states in tiny angle two dimensional semiconductors, arXiv:1901.04679.

[93] N. N. T. Nam and M. Koshino, Lattice relaxation and energy band modulation in twisted bilayer graphene, Phys. Rev. B **96**, 075311 (2017).

[94] Y. Li, H. A. Fertig, and B. Seradjeh, Floquet-engineered topological flat bands in irradiated twisted bilayer graphene, Phys. Rev. Research **2**, 043275 (2020).

[95] G. Tarnopolsky, A. J. Kruchkov, and A. Vishwanath, Origin of Magic Angles in Twisted Bilayer Graphene, Phys. Rev. Lett. **122**, 106405 (2019).

[96] Y. Yang, B. Zhen, J. D. Joannopoulos, and M. Solja i, Non-Abelian generalizations of the Hofstadter model: Spinorbit-coupled butterfly pairs, Light Sci. Appl. **9**, 177 (2020).

[97] S. Carr, S. Fang, Z. Zhu, and E. Kaxiras, Exact continuum model for low-energy electronic states of twisted bilayer graphene, Phys. Rev. Research **1**, 013001 (2019).

[98] H. Dehghani, T. Oka, and A. Mitra, Out-of-equilibrium electrons and the Hall conductance of a Floquet topological insulator, Phys. Rev. B **91**, 155422 (2015).

[99] J. D. Jackson, *Classical Electrodynamics*, 3rd ed. (Wiley, New York, NY, 1999).